Cell Reports

Report

Control of Huntington's Disease-Associated Phenotypes by the Striatum-Enriched Transcription Factor Foxp2

Graphical Abstract

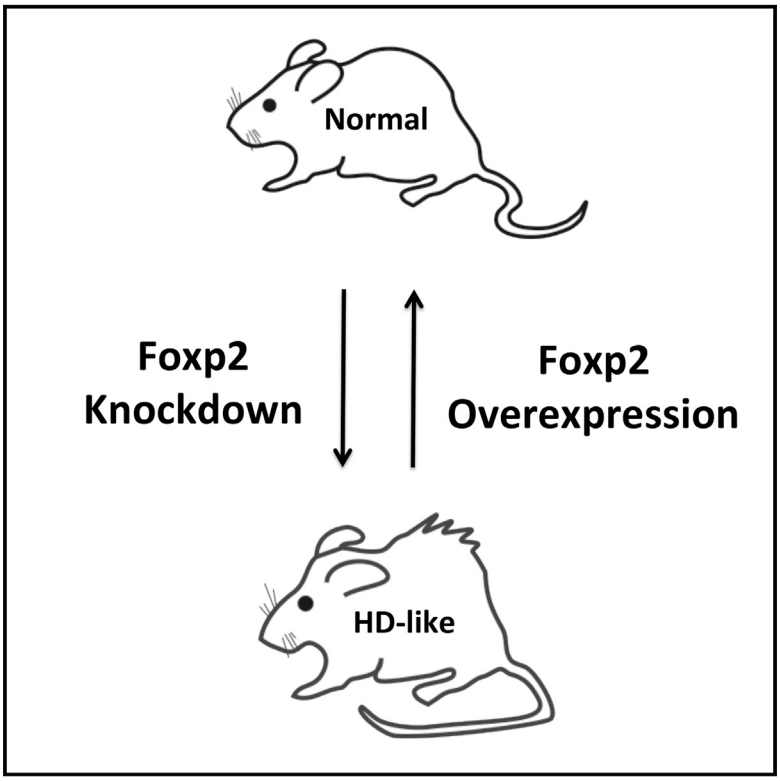

Authors

Lea J. Hachigian, Vitor Carmona, Robert J. Fenster, ..., Fan Gao, Eric D. Kolaczyk, Myriam Heiman

Correspondence

mheiman@mit.edu

In Brief

Hachigian et al. demonstrate that manipulating levels of the striatum-enriched transcription factor Foxp2 can either rescue or mimic HD-associated behaviors *in vivo*. They link Foxp2 to the post-developmental regulation of the structure and function of the corticostriatal synapse.

Highlights

- Overexpression of Foxp2 in HD model mice can rescue HD-associated behavioral deficits
- Reduction of Foxp2 levels in wild-type mice can mimic HD-associated behavioral deficits
- Foxp2 co-aggregates with mHTT in HD mouse models and human patients
- Foxp2 post-developmentally regulates genes that function at the corticostriatal synapse

Hachigian et al., 2017, Cell Reports *21*, 2688–2695
December 5, 2017
https://doi.org/10.1016/j.celrep.2017.11.018

CellPress

OPEN ACCESS
CellPress

Cell Reports
Report

Control of Huntington's Disease-Associated Phenotypes by the Striatum-Enriched Transcription Factor Foxp2

Lea J. Hachigian,[1,2,3] Vitor Carmona,[4] Robert J. Fenster,[2,9] Ruth Kulicke,[2,3] Adrian Heilbut,[3,5] Annie Sittler,[6] Luís Pereira de Almeida,[4] Jill P. Mesirov,[3,8] Fan Gao,[2] Eric D. Kolaczyk,[5,7] and Myriam Heiman[1,2,3,10,*]
[1]Department of Brain and Cognitive Sciences, MIT, Cambridge, MA 02139, USA
[2]Picower Institute for Learning and Memory, Cambridge, MA 02139, USA
[3]Broad Institute of MIT and Harvard, Cambridge, MA 02142, USA
[4]Center for Neuroscience and Cell Biology (CNC) and Faculty of Pharmacy, The University of Coimbra Rua Larga, 3004-504 Coimbra, Portugal
[5]Program in Bioinformatics, Boston University, Boston, MA 02215, USA
[6]ICM (Brain and Spine Institute) Pitié-Salpêtrière Hospital, CNRS UMR 7225, 75013 Paris, France
[7]Department of Mathematics and Statistics, Boston University, Boston, MA 02215, USA
[8]Present address: Department of Medicine, School of Medicine, UC San Diego, La Jolla, CA 92093, USA
[9]Present address: Department of Psychiatry, McLean Hospital, Harvard Medical School, Belmont, MA 02478, USA
[10]Lead Contact
*Correspondence: mheiman@mit.edu
https://doi.org/10.1016/j.celrep.2017.11.018

SUMMARY

Alteration of corticostriatal glutamatergic function is an early pathophysiological change associated with Huntington's disease (HD). The factors that regulate the maintenance of corticostriatal glutamatergic synapses post-developmentally are not well understood. Recently, the striatum-enriched transcription factor Foxp2 was implicated in the development of these synapses. Here, we show that, in mice, overexpression of Foxp2 in the adult striatum of two models of HD leads to rescue of HD-associated behaviors, while knockdown of Foxp2 in wild-type mice leads to development of HD-associated behaviors. We note that Foxp2 encodes the longest polyglutamine repeat protein in the human reference genome, and we show that it can be sequestered into aggregates with polyglutamine-expanded mutant Huntingtin protein (mHTT). Foxp2 overexpression in HD model mice leads to altered expression of several genes associated with synaptic function, genes that present additional targets for normalization of corticostriatal dysfunction in HD.

INTRODUCTION

Huntington's disease (HD) is a fatal neurodegenerative disorder caused by expansions of CAG tri-nucleotide repeats in the huntingtin (*HTT*) gene (The Huntington's Disease Collaborative Research Group, 1993). HD is characterized by motor, cognitive, and psychiatric symptoms, and spiny projection neurons (SPNs) of the caudate and putamen (striatum) are considered to be among the most vulnerable cell types in HD. HD mouse model studies have revealed early alterations to corticostriatal function and information processing in the presence of mutant Huntingtin (mHTT) (Plotkin and Surmeier, 2015). However, the molecular mechanisms underlying corticostriatal dysfunction in HD are not fully understood. As Foxp2 is expressed at high levels in both deep layer cortex and striatum (Takahashi et al., 2003), is a crucial regulator of striatal synaptogenesis and corticostriatal inputs during striatal development (Chen et al., 2016), and synaptic changes are among the earliest reported changes in HD, we tested the ability of Foxp2 overexpression to rescue HD-associated phenotypes.

RESULTS

Foxp2 Overexpression Rescues HD-Associated Behaviors in HD Model Mice

To test whether Foxp2 may post-developmentally regulate HD-associated behavioral deficits in mouse models, we overexpressed Foxp2 by adeno-associated virus (AAV)-mediated transduction (Figure 1A). BACHD model mice and their isogenic controls were injected bilaterally in the dorsal striatum either with a Foxp2 overexpression vector under the EF1a promoter (Foxp2 overexpression [OX]) or control AAV9 construct and then were subjected to a series of behavioral assays (Figure 1B). We observed viral spread in the dorsal striatum and, to a much lesser extent, the deep layer cortex and preferential infection of neurons over astrocytes using NeuN and Sox9 as markers (Sun et al., 2017) (Figures S1A and S1E). Injections did not result in aberrant astrocyte or microglial activation (Figures S1C and S1D). Foxp2 OX increased Foxp2 protein levels in the striatum of these BACHD mice by 2.3-fold (Figure S1F). While control virus-injected BACHD mice showed hypoactivity in an open field assay compared to control virus-injected wild-type animals (mean 18,307.7 cm in controls versus 12,565.0 cm in BACHD), Foxp2 OX fully reversed this phenotype (mean 17,514.3 cm) (Figure 1C). Previously reported HD model deficits in grip strength (Menalled et al., 2009) were recapitulated (mean

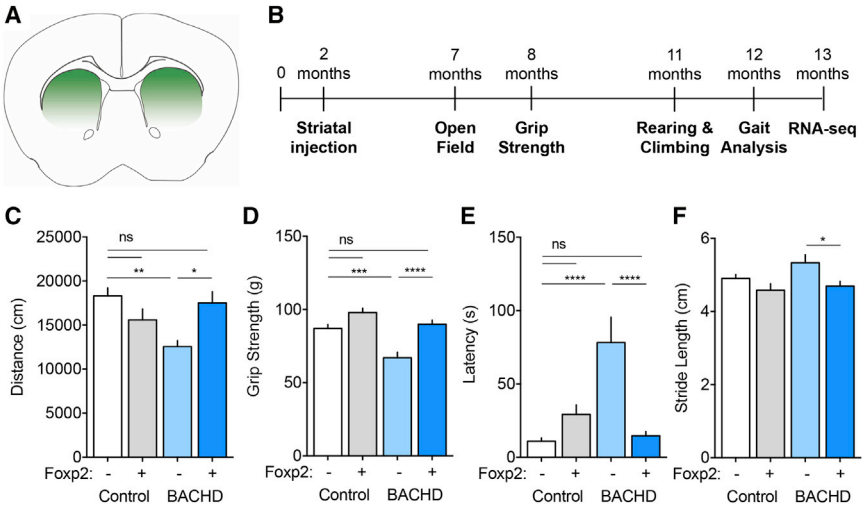

Figure 1. Post-developmental Striatal Foxp2 Overexpression Rescues HD-Associated Behaviors in the BACHD Model

(A) Schematic depiction of striatal-targeted Foxp2 overexpression (OX) and control virus injections into the dorsal striatum.

(B) Timeline of injections and behavioral testing in BACHD and control mice with Foxp2 manipulation.

(C) Open field horizontal distance traveled (cm) in a 1-hr testing period at 7 months (n = 15 [Con + Con]; n = 13 [Con + Foxp2]; n = 12 [BACHD + Con]; n = 15 [BACHD + Foxp2]).

(D) Grip strength (maximum g force) at 8 months (n = 18 [Con + Con and Con + Foxp2]; n = 16 [BACHD + Con and BACHD + Foxp2]).

(E) Latency (seconds) for mice to rear in a 5-min testing period (n = 14 [Con + Con and Con + Foxp2]; n = 12 [BACHD + Con and BACHD + Foxp2]).

(F) Gait stride length measurements (cm) (n = 13 [Con + Con and Con + Foxp2]; n = 11 [BACHD + Con]; n = 12 [BACHD + Foxp2]). All error bars: mean + SEM. Overbar endpoints denote pairwise comparisons. *p < 0.05, **p < 0.01, ***p < 0.001, ****p < 0.0001; one-way ANOVA (significance cutoff p < 0.05) with Bonferroni correction across all means.

See also Figure S1.

87.0 g in controls versus 67.0 g in BACHD) (Figure 1D) and Foxp2 OX rescued this deficit to control levels (mean 89.9 g) (Figure 1D). Control BACHD mice showed deficits in rearing (mean latency 11.0 s in controls versus 78.2 s in BACHD) (Figure 1E) and vertical cage exploration (mean latency 22.7 s in controls versus 95.3 s in BACHD) (Figure S1G) that were also reversed to control levels with Foxp2 OX (mean 14.7 s and mean 26.0 s, respectively) (Figures 1E and S1G). A range of gait deficits have been reported in BACHD model mice, (Menalled et al., 2009) and we observed differences between BACHD mice and littermate controls in stride length, base length, and splay (Figures 1F, S1H, and S1I). Striatal Foxp2 OX produced trends toward phenotypic rescue in stride base length and splay and a significant rescue of the stride length (mean 5.3 cm in control-injected BACHD versus 4.7 cm in Foxp2-injected BACHD) (Figure 1F). Finally, to test the effect of Foxp2 OX in an advanced symptomatic and rapidly progressing model of HD, we performed similar bilateral dorsal striatal Foxp2 OX injections into the more phenotypically severe R6/2 mouse model of HD (Mangiarini et al., 1996). Striatal Foxp2 OX in symptomatic R6/2 mice significantly improved vertical activity in the open field (mean 36.4 counts in control-injected R6/2 versus 94.2 counts in Foxp2-injected R6/2) (Figure S1J) and also led to an increase in rearing and climbing activity compared to control-injected R6/2 mice (mean 5.7 episodes in control-injected R6/2 versus 11.4 episodes in Foxp2-injected R6/2) (Figure S1K). Moreover, Foxp2 OX produced a significant improvement in rotarod performance in these mice relative to control-injected mice (Figure S1L). Thus, although Foxp2 OX was induced in the R6/2 animals at a post-symptomatic time point (6 weeks of age), this manipulation was able to achieve significant rescue of various HD-associated phenotypes in a severe phenotypic model. Taken together, our results demonstrate that increased Foxp2 expression in the striatum, likely by restoring synaptic function, can rescue HD-associated behavioral deficits, even in a severe phenotypic model.

Foxp2 Post-developmentally Regulates the Corticostriatal Synapse

Although Foxp2 is a transcription factor, previous studies have not examined post-developmental Foxp2 gene targets (Spiteri et al., 2007; Vernes et al., 2007, 2011). Thus, we next assayed which gene targets might underlie the behavioral rescue we observed upon Foxp2 overexpression in HD models. Striatal RNA from BACHD and control animals was isolated at 13 months of age and was used for RNA sequencing (RNA-seq) followed by differential gene expression analysis (n = 4 mice per group, adjusted p value < 0.05). In the context of mutant Huntingtin (mHTT) alone, BACHD versus control animals displayed only a small number of changes to striatal gene expression (Figure S2; Table S1), consistent with previous reports for some other full-length mHTT models (Mazarei et al., 2010). Analysis of RNA-seq data of the Foxp2 OX versus control group revealed that striatal Foxp2 regulates the expression of several genes involved in synapse function and formation post-developmentally (Figures 2A, 2B, and S2; Table S1). Several of these genes were similarly altered in the BACHD model upon Foxp2 OX (Figures 2C, 2D, and S2; Table S1), indicating that Foxp2 OX in an HD context can also alter expression of genes whose products function at the synapse. Further, these gene expression data identify a small set of striatal-expressed genes that mediate the therapeutic effects of Foxp2 OX in the BACHD models. Of particular interest is downregulation of *Pde2a*, which, like *Pde10a*, encodes a striatal-enriched cyclic AMP (cAMP) and cyclic guanosine monophosphate (cGMP) dual phosphodiesterase (Menniti et al., 2006). As Pde10a inhibition recently has shown promise as a therapeutic target in HD models (Beaumont et al., 2016), but alone may not be sufficient for HD symptom rescue in patients, our data suggest that the use of selective Pde2a inhibitors (Gomez and Breitenbucher, 2013) may also have therapeutic potential. Our data show that a gene with the most altered expression in the BACHD model versus control is *Actn2* (Figure S2B; Table S1), a gene that has previously been shown to be altered

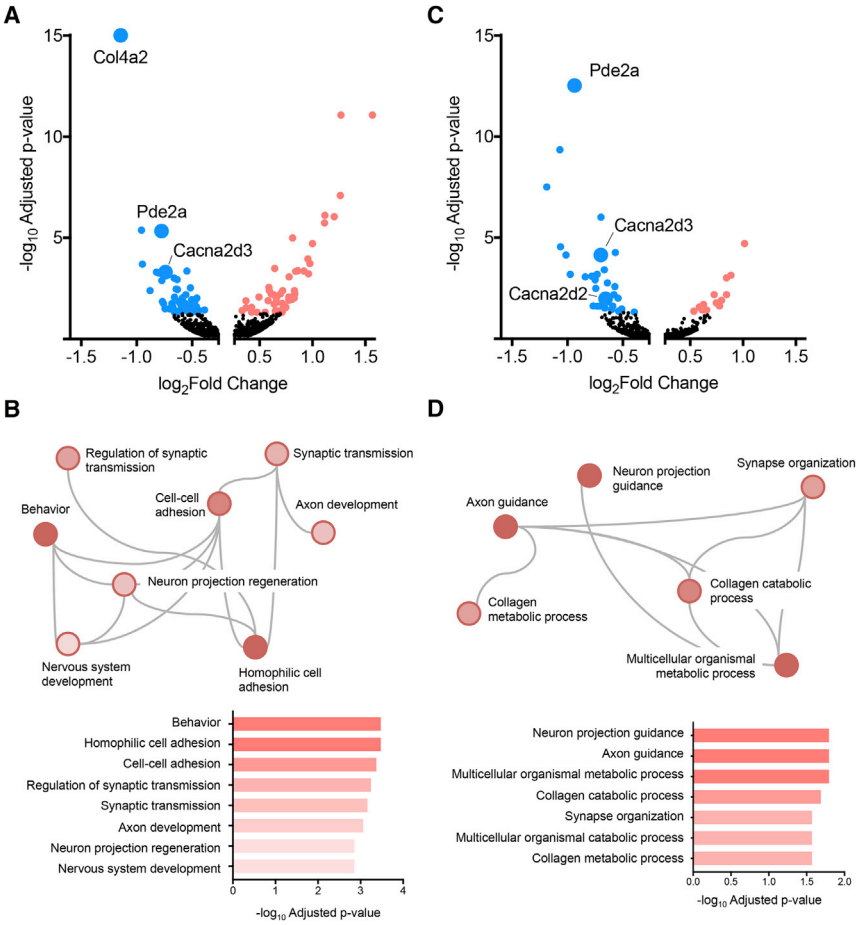

Figure 2. Striatal Foxp2 Post-developmentally Regulates Genes Involved in Synapse Function and Formation

(A and C) Differentially expressed genes upon Foxp2 overexpression in control mice (A) and Foxp2 overexpression in BACHD mice (C). Significant genes (adjusted p value < 0.05) are highlighted in red (upregulated) or blue (downregulated). Cut-offs of ±1.2-fold change and p value < 0.05 used for display purposes.

(B and D) Gene ontology analysis of genes changed in control (B) or BACHD (D) mice with Foxp2 overexpression. Coloring is proportional to adjusted p value.

See also Figure S2 and Table S1.

in HD and mouse models (Lee et al., 2013; Mazarei et al., 2010) and has been implicated in the regulation of both dendritic spine morphology and NMDA receptor inactivation. Foxp2 OX in the BACHD model induced changes to a known Rho-signaling pathway modulator (the guanine nucleotide exchange factor *Mcf2l*) (Figure S2H; Table S1) and voltage-gated calcium channel modulatory subunits (*Cacna2d2* and *Cacna2d3*) (Figures S2E and S2F; Table S1). Thus, it is possible that these changes to *Mcf2l*, *Cacna2d2*, and *Cacna2d3* expression may reflect a compensation to the decreased *Actn2* levels induced by mHTT, given the known roles of Rho signaling in regulation of dendritic spine morphology and of dendritic voltage-gated calcium channels in synaptic calcium entry; however, further studies will be needed to test this hypothesis and make mechanistic predictions. The decreases in expression of *Dgkz* and *Dgki*, two diacylglycerol kinases, predicted an increase to protein kinase C activity (Yang et al., 2011) upon Foxp2 OX. The AMPAR subunit GluR2 is phosphorylated by PKC at serine-880 (Chung et al., 2000), and we observed an increase in this residue's phosphorylation with Foxp2 OX in BACHD mice (Figure S2I), a change that may lead to increased calcium influx at the synapse (via internalization of calcium impermeable GluR2-containing AMPA receptor subunits) (Isaac et al., 2007; Park et al., 2009). Additionally, as a general marker of corticostriatal connections, we tested PSD95 levels and observed an increase with Foxp2 OX in BACHD mice (Figure S2J). Further experiments will be needed to test the relative contributions of each of these changes to the therapeutic benefit of Foxp2 OX. Given the pleiotropic effects of mHTT (Zuccato et al., 2010), it is possible that several pathway changes, all impacted by Foxp2 OX, are needed for the full motor phenotypic rescue that we observed in the BACHD model.

Lowering Foxp2 Levels *In Vivo* Reproduces HD-Associated Behaviors

We next tested the consequences of lowering Foxp2 levels (Foxp2 knockdown, KD) in wild-type adult striatum by injection of an AAV9-short hairpin RNA (shRNA) construct targeting Foxp2 under a U6 promoter (Figures 3A and S1B) and assessing HD-relevant behaviors (Figure 3B). With this manipulation, we observed a stable decrease in Foxp2 protein levels at both two and four weeks post-injection (mean 0.7 and 0.6, respectively, in KD normalized to control) (Figure S3A) and as upon Foxp2 OX, did not observe microglial or astroglial activation (data not shown). Mice with striatal Foxp2 KD displayed a significant decrease in latency to fall versus control shRNA-injected wild-type mice on an accelerating rotarod test (183.0 s in Foxp2 KD versus 244.0 s in controls on first day of testing) (Figure 3C). In addition, Foxp2 KD mice also displayed an increase in training falls compared to controls on this test (mean 0.4 in controls versus 1.1 in Foxp2 KD) (Figure 3D). Foxp2 KD mice showed a significant and persistent reduction in vertical activity in the open field assay (mean 1,037.3 counts in controls versus 771.1 counts in Foxp2 KD at 5 weeks; mean 977.7 counts in controls versus 804.8 counts in Foxp2 KD at 10 weeks) (Figures 3E and S3B). This effect was coupled with a reduction in rearing and climbing events (mean 34.0 events in controls versus 21.4 events in Foxp2 KD) (Figure 3F). Foxp2 KD mice showed increased latencies in the initiation of both rearing and vertical cage exploration (mean 8.9 s in controls versus 43.3 s in Foxp2 KD; mean 14.6 s in controls

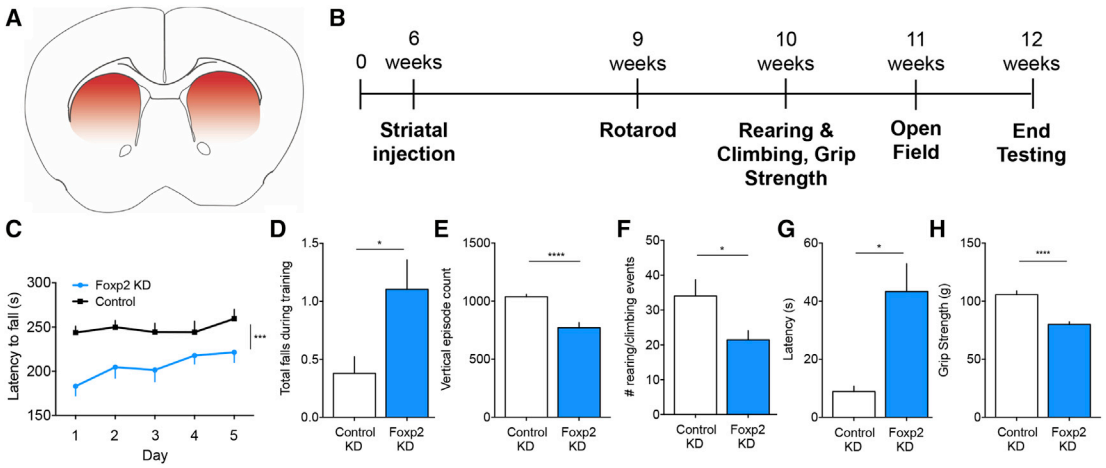

Figure 3. Post-developmental Striatal Foxp2 Knockdown Produces HD-Associated Behaviors

(A) Schematic depiction of striatal-targeted Foxp2 knockdown (KD) and control virus injections into the dorsal striatum.

(B) Timeline of injections and behavioral testing in Foxp2 KD and control mice.

(C) Accelerating rotarod performance (latency to fall, seconds), n = 19 per group.

(D) Falls during rotarod training trial, n = 10 per group.

(E) Open field vertical episode count in a 1-hr testing period, n = 9 per group.

(F) Total rearing and climbing events in a 5-min testing period, n = 9 per group.

(G) Latency (seconds) for mice to rear in a 5-min testing period, n = 10 control and n = 20 Foxp2 KD mice.

(H) Grip strength (maximum g force), n = 10 control, n = 20 Foxp2 KD mice. All error bars: mean ± SEM. Overbar endpoints denote pairwise comparisons. ns, not significant, *p < 0.05, **p < 0.01, ***p < 0.001, ****p < 0.0001; repeated-measures ANOVA and two-tailed t test.

See also Figure S3.

versus 81.6 s in Foxp2 KD) (Figures 3G and S3C). We also observed a large deficit in grip strength in these mice (mean 105.7 g in controls compared to 80.0 g in Foxp2 KD) (Figure 3H). Similar rotarod performance deficits and reduced activity measurement were seen with a second, independent Foxp2 shRNA KD virus (Figures S3D and S3E). Together, these data show that Foxp2 KD can itself alone recapitulate various HD-associated motor phenotypes and thus provide further evidence that the genes that are under the regulatory control of Foxp2 have functional significance to HD-associated phenotypes.

Foxp2 Co-aggregates with Mutant Huntingtin Protein

Given these OX and KD findings, to determine whether the endogenous Foxp2 protein is perturbed in HD, we first examined its protein sequence and noted that *FOXP2* encodes the longest polyglutamine repeat protein in the human reference genome, with 40 continuous polyglutamine repeats (compared to normal *HTT* at 23 repeats, Table S2). Although *FOXP2* striatal gene expression has not been reported to be altered in human HD gene expression studies (Hodges et al., 2006), there is evidence that Foxp2 interacts with the HTT protein (Shirasaki et al., 2012; Li et al., 2016). We therefore tested to what extent Foxp2 co-aggregates with mutant mHTT *in vivo*. Samples from the caudate nucleus and putamen of stage III/IV human HD post-mortem brain showed a significant loss of soluble FOXP2 protein by western blotting (Figure 4A), consistent with co-aggregation with mHTT into insoluble aggregates. We tested expression and localization of Foxp2 in HD mouse model tissue to determine whether levels of soluble Foxp2 change and whether Foxp2 co-aggregates with mHTT *in vivo*. R6/2 mice showed an almost complete loss of soluble Foxp2 protein in the striatum, as compared to their isogenic controls and measured by western blot analysis (11.5 weeks of age, mean 0.1 in R6/2 normalized to controls) (Figure 4B). A decrease in Foxp2 mRNA expression changes could not account for the loss of soluble Foxp2 in R6/2 animals, as only a small decrease in Foxp2 mRNA was observed from samples taken from the same mice (Figure S4A). Examining the BACHD model, we also detected a slight loss of soluble striatal Foxp2 protein by western blot analysis (13 months of age, mean 0.8 in BACHD normalized to controls) (Figure 4B). To test whether this loss of soluble Foxp2 levels in HD model tissue correlated with an increase in aggregation, we examined the localization of Foxp2 at a sub-cellular level using indirect immunofluorescence in R6/2 striatal tissue sections. In isogenic control mice, Foxp2 was localized diffusely throughout the nucleus of striatal neurons, whereas similar immunostaining in R6/2 tissue showed a clear pattern of Foxp2 co-aggregation with mHTT (Figure 4C). Foxp2 OX in R6/2 animals restored diffuse nuclear expression of Foxp2 alongside the Foxp2 co-aggregation with mHTT (Figure S4C). We also observed co-aggregation of Foxp2 with mHTT in the zQ175 knockin model of HD, which expresses full-length mHTT with ~190 CAG repeats (Figure 4D). Finally, in order to determine Foxp2 co-aggregation with mutant expanded polyglutamine-stretch proteins that do or do not lead to striatal pathology or dysfunction, we examined striatal tissue from spinocerebellar ataxia 3 (SCA3; has striatal involvement) and spinocerebellar ataxia 7 (SCA7; no reported striatal involvement) model mice. Even though SCA7 model mice (Yoo et al., 2003) showed clear aggregation of mutant Ataxin7 protein in the striatum, Foxp2 retained its normal nuclear expression

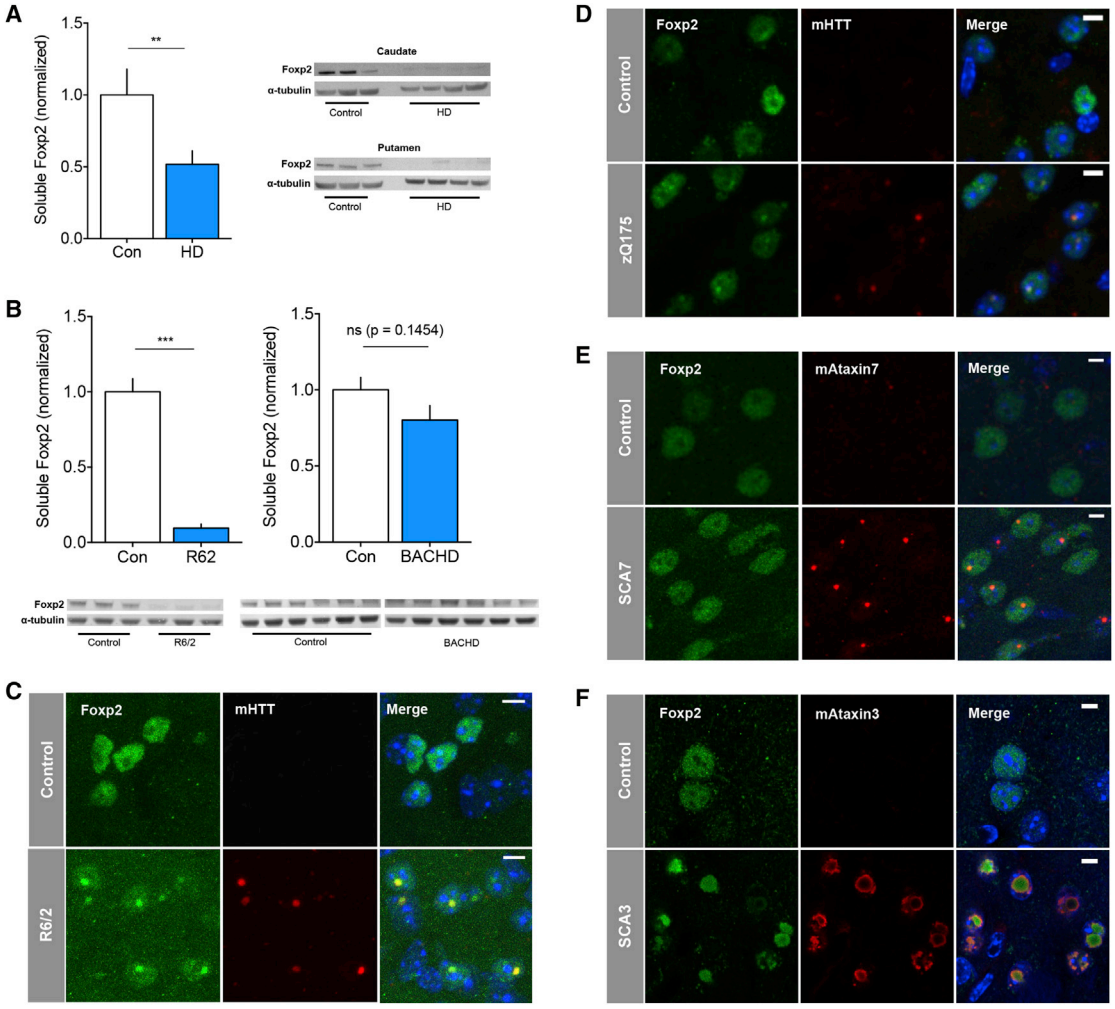

Figure 4. Soluble Foxp2 Protein Levels Are Decreased in HD and HD Model Tissue, and Foxp2 Co-aggregates with mHTT and mAtaxin3, but Not mAtaxin7

(A) Soluble Foxp2 levels in 4 human HD patients (grade 3/4) and 3 age and post-mortem interval-matched controls.

(B) Soluble Foxp2 levels in R6/2 (left) and BACHD (right) HD mouse model striatal tissue. n = 3 R6/2 mice and littermate controls at 11.5 weeks of age. n = 6 BACHD mice and littermate controls at 13 months of age. Data plotted as normalized versus beta-actin.

(C) Indirect immunofluorescence to Foxp2 in R6/2 and isogenic control striatal tissue at 12 weeks of age; mHTT aggregates stained with antibody EM48.

(D) Indirect immunofluorescence to Foxp2 in zQ175 knockin and isogenic control striatal tissue at 10.5 months of age; mHTT aggregates stained with antibody EM48.

(E) Indirect immunofluorescence to Foxp2 in SCA7 mutant and isogenic control striatal tissue at 9 months of age.

(F) Indirect immunofluorescence to Foxp2 in SCA3 mutant-injected and isogenic control striatal tissue at 4 weeks post mutant Ataxin3 injection. DAPI signal pseudocolored in blue in the merge signal (C–F). Scale bars, 5 μm. All error bars, mean + SEM. Overbar endpoints denote pairwise comparisons. ns, not significant. **$p < 0.01$, ***$p < 0.001$; two-tailed t test.

See also Figure S4 and Table S2.

pattern and was not found to co-aggregate (Figure 4E). In contrast, we observed Foxp2 co-aggregation with mutant Ataxin3 (Alves et al., 2008) in the striatum (Figure 4F). It is interesting to note that in the latter case, Foxp2 aggregates appeared to be surrounded by mutant Ataxin3, as opposed to what appeared to be strict Foxp2 co-localization with mHTT aggregates. These data collectively demonstrate that soluble Foxp2 levels are depleted to great extent in HD and HD model tissue and further suggest that Foxp2 aggregation may be a characteristic of mutant expanded polyglutamine proteins that cause striatal pathology or dysfunction (mHTT or mutant Ataxin3).

DISCUSSION

Our data show that reductions to striatal Foxp2 levels can produce HD-associated behavioral phenotypes. We show that Foxp2 can co-aggregate with mHTT and mutant Ataxin3, two pathogenic proteins that cause striatal cell death or dysfunction,

but not mutant Ataxin7, a protein that is not linked to striatal cell death or dysfunction. Foxp2 overexpression can rescue HD-associated phenotypes in two mouse models of HD, and by RNA-seq, we further identify a small group of striatum-expressed genes that underlie the therapeutic effects of Foxp2 overexpression in HD models.

The developmental functions of Foxp2, a transcription factor of the forkhead-box family, have been well studied due to the association of Foxp2 with a genetic speech and language disorder (Lai et al., 2001). Foxp2 targets in the developing brain include several genes involved in signaling cascades, neurite outgrowth and development, as well as regulation of axonal morphology (Spiteri et al., 2007; Vernes et al., 2011), and recent studies in cultured cells also suggest that Foxp2 may interact more specifically with retinoic acid signaling pathways (Devanna et al., 2014). The targets of Foxp2 in the embryonic mouse brain collectively identified in these studies suggested a role for Foxp2 in the regulation of genes involved in remodeling of neuronal connections in the adult brain (Spiteri et al., 2007), a prediction that is borne out by our findings.

Studies *in vitro* have indicated that large mHTT inclusions can be neuroprotective (Arrasate et al., 2004), and studies in the R6/2 model indicate that the presence of neuronal mHTT intranuclear inclusions may not correlate with transcriptional dysregulation (Sadri-Vakili et al., 2006). Given that soluble forms of mHTT can also alter polyQ-rich transcription factor activity (Dunah et al., 2002), an import question will be to understand how Foxp2 binding to DNA is altered both during HD progression and in the context of different aggregate species of mHTT.

Corticostriatal glutamatergic functional abnormalities have been described as early features of HD model progression and there is pre-clinical evidence showing that normalization of corticostriatal function may have therapeutic potential for treating HD. However, it is important to note that previous therapeutic strategies targeted to normalize glutamatergic corticostriatal function in HD models have focused on the functional modulation of individual protein function, for example Pde10a (Beaumont et al., 2016), one among many recent protein targets with HD relevance. None of these individual targets has so far showed success in symptom amelioration in a clinical setting, and indeed studies in HD model mice suggest that normalization of distinct glutamatergic corticostriatal functional abnormalities is necessary but not sufficient for rescue of HD-associated motor symptomatology. Due to: (1) extent of the HD-associated phenotypic rescue that we have observed upon Foxp2 overexpression, (2) the fact that Foxp2 overexpression regulates pleiotropic gene targets that act at the corticostriatal synapse, and (3) that mHTT itself likely has pleiotropic effects at the synapse, we hypothesize that a "pleiotropic regulator" target strategy, rather than an individual target strategy, may hold great promise for future HD therapeutic strategies. Given the relatively small number of genes modulated by Foxp2 for HD model rescue and that several of these genes' products (Cacna2d2, Pde2a, and Mcf2l) have known direct or indirect pharmacological inhibitors, testing this hypothesis is an important goal for future studies.

EXPERIMENTAL PROCEDURES

Experimental Samples

All animal experiments were conducted with the approval of the Massachusetts Institute of Technology Animal Care and Use Committee. Mice were housed with food and water provided *ad libitum* on a standard 12 hr light/12 hr dark cycle. Only male mice were used given HD model gender differences in phenotype progression.

BACHD mice (Gray et al., 2008) were used at 2–13 months of age. R6/2 mice (Mangiarini et al., 1996) were used at 5–12 weeks of age. zQ175 male mice (Menalled et al., 2003) were used at 10.5 months of age. C57BL/6J male mice 8–24 weeks of age were used for wild-type Foxp2 knockdown studies. SCA7 mice (Yoo et al., 2003) were used at 9 months of age and SCA3 male model mice (Alves et al., 2008) were used starting at 5 weeks of age.

Human HD postmortem brain samples were obtained from the Human Brain and Spinal Fluid Resource Center at UCLA. Samples were all classified as grades 3 or 4 for both the caudate nucleus and putamen. Age, post-mortem interval, and region-matched controls were obtained from the Alabama Brain Collection at University of Alabama at Birmingham, Alabama.

Surgical Injection of AAV Foxp2 Viruses

Coordinates for bilateral striatal AAV injection were as follows: anterior-posterior = 0.6, medial-lateral = +/−1.85, and dorsal-ventral = −3.5 (in mm relative to Bregma). Foxp2 overexpression constructs were packaged into AAV9 vectors (Virovek, Hayward, CA) as the following completed virus: AAV9-EF1α -FoxP2-Myc-DDK-WPRE using Foxp2 NM_014491. Foxp2 knockdown constructs were also packaged into AAV9 vectors (SignaGen, Rockville MD) as the following completed virus: ITR-U6-shRNA(Foxp2)-Ef1α-GFP-PolyA-ITR. The first Foxp2 target shRNA sequence was 5′-GCAACAGTTCAATGAATCAAA-3′, and the second was 5′-GCGACATTCAGACAAATACAA-3′. shRNA scramble controls were also used (SignaGen, Rockville MD) with the same construction: ITR-U6-shRNA(Scramble)-Ef1α-GFP-PolyA-ITR.

Behavioral Testing

Behavioral outliers ±2 SD from the mean were removed from analyses. Open field testing was performed in one 60-min session per mouse using an infrared (IR) photobeam open field (17″ × 17″ × 12″) with 16 IR beams spaced regularly along the x, y, and z axes (#MED-OFAS-RSU, Med Associates, St. Albans, VT). Grip strength testing was performed using a grip strength meter (Ugo Basile, Varese, Italy). Mice were suspended by their tails and allowed to grab onto the measurement bar. They were then slowly pulled away from the bar by the tail until they released the bar and the maximum force (g) was recorded. Each mouse was given 5 trials.

Rearing and climbing testing was performed by placing mice underneath an overturned metal mesh pencil cup (Rolodex #82406) 4.375 inches in diameter and 5.5 inches in height. The latency until the mouse reared on hind legs alone without touching the mesh and the latency until the mouse put both front paws up onto the mesh were recorded. Mice were given one 5-min trial. Gait analysis was performed as described in Menalled et al. (2009). Briefly, mice had their hind paws painted with one color of nontoxic paint and their front paws painted with a different color of nontoxic paint. They were permitted to walk along white paper and footprints were measured for stride length, base length, and splay. An average of 3 consecutive step measurements was taken for each mouse. Rotarod testing was performed using an accelerating rotarod (Ugo Basile, Varese, Italy). Mice were trained using 3 × 5 min sessions with a fixed speed of 20 rotations per minute (RPM) and replaced on the rotarod after each fall. Mice were given 1 min of rest between training trials. Testing was performed on 5 consecutive days with the rotarod accelerating from 5 RPM to 40 RPM over the course of 5 min. The time from the start of the trial until the mouse fell off the rod was measured as latency to fall. If a mouse completed two or more passive rotations, this was scored as a fall. As previously reported, BACHD mice in our colony displayed a substantial weight gain that precluded rotarod testing (Kudwa et al., 2013).

Indirect Immunofluorescence

Samples were prepared for immunofluorescence by transcardial perfusion followed by tissue processing and staining as previously described (Heiman

et al., 2008). Antibodies used are listed in the Supplemental Experimental Procedures.

Western Blotting

Mouse and human striatal tissues were dissected and flash frozen in liquid nitrogen. Tissue was sonicated in 750 μL of 1% SDS with Halt protease and phosphatase inhibitors (ThermoScientific, Rockford, IL) using a Branson sonicator (Branson Ultrasonics, Danbury, CT) at 25% amplitude for two sessions of 15 s, with 30 s between trials on ice. Antibodies used are listed in the Supplemental Experimental Procedures.

qRT-PCR

Mouse striatal tissue was dissected and flash frozen in liquid nitrogen. Tissue was disrupted for RNA isolation using the TissueLyser (QIAGEN, Hilden, Germany) for 2 × 2 min at 25 Hz as recommended by the manufacturer. RNA was then isolated using the RNeasy Lipid Tissue Mini Kit (QIAGEN, Hilden, Germany). For qRT-PCR, the TaqMan Universal Master Mix (ThermoScientific, Rockford, IL) was used, and PCR reactions were run on a StepOnePlus system (ThermoScientific, Rockford, IL). Probes used are listed in the Supplemental Experimental Procedures.

RNA-Seq and Analysis

Samples were prepared for RNA-seq using the Clontech SMARTer total RNA-seq kit (Takara, Mountain View, CA). The quality of prepared bar-coded libraries was assessed using an Advanced Analytical-fragment Analyzer (Advanced Analytical, Ankeny, IA) before mixing for sequencing on the Illumina HiSeq 2000 (Illumina, San Diego, CA) platform at the MIT BioMicro Center. The raw fastq data of 50-bp single-end sequencing reads were aligned to the mouse mm10 reference genome using the STAR 2.4.0 RNA-seq aligner (Dobin et al., 2013). The mapped reads were processed by htseq-count of HTSeq software (Anders et al., 2015) with mm10 gene annotation to count the number of reads mapped to each gene. Gene differential expression test between different animal groups was performed using DESeq2 package (Love et al., 2014) with the assumption of negative binomial distribution for RNA-seq data. Genes with adjusted p value < 0.05 were chosen as differentially expressed genes. For gene ontology (GO) and pathway analyses, differentially expressed genes were processed using Enrichr (Chen et al., 2013; Kuleshov et al., 2016).

Statistical Analyses

Statistical analyses for all behavioral data, qPCR, and western blot quantification were performed in Prism 7. For all comparisons of two groups, an unpaired t test was used to assess significance with a cutoff of <0.05 for significance. All t tests were two-tailed except for the tests in Figures S2I and S2J, as directionality of change was expected. For all comparisons of four BACHD testing groups, two-way ANOVA with a Bonferroni post-test (comparing the mean of each group to the mean of every other group) was used with a cutoff of <0.05 for significance. For rotarod data, repeated-measures ANOVA with genotype + virus as the comparison factor was used with a cutoff of <0.05 for significance. N is the number of mice is reported in each figure legend. Means are reported in the text. Error bars represent mean value plus SEM. Overbar endpoints denote comparisons (*p < 0.05, **p < 0.01, ***p < 0.001, and ****p < 0.0001 for all figures). Behavioral outliers ± 2 SDs from the mean were removed from analyses. For RNA-seq, a cutoff of p adjusted <0.05 was used to determine significance.

DATA AND SOFTWARE AVAILABILITY

The accession number for the RNA-seq data reported in this study is GEO: 104990.

SUPPLEMENTAL INFORMATION

Supplemental Information includes Supplemental Experimental Procedures, four figures, and two tables and can be found with this article online at https://doi.org/10.1016/j.celrep.2017.11.018.

AUTHOR CONTRIBUTIONS

L.J.H. performed experiments and analyses and drafted the paper. V.C. and L.P.d.A. performed all SCA3 experiments. R.J.F. and R.K. performed pilot experiments. A.H., J.P.M., and E.D.K. provided statistical analysis of polyQ repeats in the genome. A.S. prepared and provided SCA7 tissue. F.G. analyzed the RNA-seq data. M.H. supervised the project and revised the manuscript. All authors reviewed and approved the final manuscript.

ACKNOWLEDGMENTS

The authors gratefully acknowledge the Human Brain and Spinal Fluid Resource Center at UCLA and the Alabama Brain Collection at the University of Alabama at Birmingham for providing tissue samples. This work was supported by generous gifts from the Lock/Chin family (to M.H.) and Latham family (to M.H.), an award from the JPB Foundation (to M.H.), and an NSF predoctoral fellowship (to L.H.).

Received: June 9, 2017
Revised: September 19, 2017
Accepted: November 2, 2017
Published: December 5, 2017

REFERENCES

Alves, S., Régulier, E., Nascimento-Ferreira, I., Hassig, R., Dufour, N., Koeppen, A., Carvalho, A.L., Simões, S., de Lima, M.C.P., Brouillet, E., et al. (2008). Striatal and nigral pathology in a lentiviral rat model of Machado-Joseph disease. Hum. Mol. Genet. *17*, 2071–2083.

Anders, S., Pyl, P.T., and Huber, W. (2015). HTSeq–a Python framework to work with high-throughput sequencing data. Bioinformatics *31*, 166–169.

Arrasate, M., Mitra, S., Schweitzer, E.S., Segal, M.R., and Finkbeiner, S. (2004). Inclusion body formation reduces levels of mutant huntingtin and the risk of neuronal death. Nature *431*, 805–810.

Beaumont, V., Zhong, S., Lin, H., Xu, W., Bradaia, A., Steidl, E., Gleyzes, M., Wadel, K., Buisson, B., Padovan-Neto, F.E., et al. (2016). Phosphodiesterase 10A inhibition improves cortico-basal ganglia function in Huntington's disease models. Neuron *92*, 1220–1237.

Chen, E.Y., Tan, C.M., Kou, Y., Duan, Q., Wang, Z., Meirelles, G.V., Clark, N.R., and Ma'ayan, A. (2013). Enrichr: interactive and collaborative HTML5 gene list enrichment analysis tool. BMC Bioinformatics *14*, 128.

Chen, Y.-C., Kuo, H.-Y., Bornschein, U., Takahashi, H., Chen, S.-Y., Lu, K.-M., Yang, H.-Y., Chen, G.-M., Lin, J.-R., Lee, Y.-H., et al. (2016). Foxp2 controls synaptic wiring of corticostriatal circuits and vocal communication by opposing Mef2c. Nat. Neurosci. *19*, 1513–1522.

Chung, H.J., Xia, J., Scannevin, R.H., Zhang, X., and Huganir, R.L. (2000). Phosphorylation of the AMPA receptor subunit GluR2 differentially regulates its interaction with PDZ domain-containing proteins. J. Neurosci. *20*, 7258–7267.

Devanna, P., Middelbeek, J., and Vernes, S.C. (2014). FOXP2 drives neuronal differentiation by interacting with retinoic acid signaling pathways. Front. Cell. Neurosci. *8*, 305.

Dobin, A., Davis, C.A., Schlesinger, F., Drenkow, J., Zaleski, C., Jha, S., Batut, P., Chaisson, M., and Gingeras, T.R. (2013). STAR: ultrafast universal RNA-seq aligner. Bioinformatics *29*, 15–21.

Dunah, A.W., Jeong, H., Griffin, A., Kim, Y.M., Standaert, D.G., Hersch, S.M., Mouradian, M.M., Young, A.B., Tanese, N., and Krainc, D. (2002). Sp1 and TAFII130 transcriptional activity disrupted in early Huntington's disease. Science *296*, 2238–2243.

Gomez, L., and Breitenbucher, J.G. (2013). PDE2 inhibition: potential for the treatment of cognitive disorders. Bioorg. Med. Chem. Lett. *23*, 6522–6527.

Gray, M., Shirasaki, D.I., Cepeda, C., André, V.M., Wilburn, B., Lu, X.-H., Tao, J., Yamazaki, I., Li, S.-H., Sun, Y.E., et al. (2008). Full-length human mutant

huntingtin with a stable polyglutamine repeat can elicit progressive and selective neuropathogenesis in BACHD mice. J. Neurosci. *28*, 6182–6195.

Heiman, M., Schaefer, A., Gong, S., Peterson, J.D., Day, M., Ramsey, K.E., Suárez-Fariñas, M., Schwarz, C., Stephan, D.A., Surmeier, D.J., et al. (2008). A translational profiling approach for the molecular characterization of CNS cell types. Cell *135*, 738–748.

Hodges, A., Strand, A.D., Aragaki, A.K., Kuhn, A., Sengstag, T., Hughes, G., Elliston, L.A., Hartog, C., Goldstein, D.R., Thu, D., et al. (2006). Regional and cellular gene expression changes in human Huntington's disease brain. Hum. Mol. Genet. *15*, 965–977.

Isaac, J.T.R., Ashby, M.C., and McBain, C.J. (2007). The role of the GluR2 subunit in AMPA receptor function and synaptic plasticity. Neuron *54*, 859–871.

Kudwa, A.E., Menalled, L.B., Oakeshott, S., Murphy, C., Mushlin, R., Fitzpatrick, J., Miller, S.F., McConnell, K., Port, R., Torello, J., et al. (2013). Increased body weight of the BAC HD transgenic mouse model of Huntington's Disease accounts for some but not all of the observed HD-like motor deficits. PLoS Curr. *5*, ecurrents.hd.0ab4f3645aff523c56ecc8ccbe41a198.

Kuleshov, M.V., Jones, M.R., Rouillard, A.D., Fernandez, N.F., Duan, Q., Wang, Z., Koplev, S., Jenkins, S.L., Jagodnik, K.M., Lachmann, A., et al. (2016). Enrichr: a comprehensive gene set enrichment analysis web server 2016 update. Nucleic Acids Res. *44* (*W1*), W90-7.

Lai, C.S., Fisher, S.E., Hurst, J.A., Vargha-Khadem, F., and Monaco, A.P. (2001). A forkhead-domain gene is mutated in a severe speech and language disorder. Nature *413*, 519–523.

Lee, C.Y.D., Cantle, J.P., and Yang, X.W. (2013). Genetic manipulations of mutant huntingtin in mice: new insights into Huntington's disease pathogenesis. FEBS J. *280*, 4382–4394.

Li, L., Liu, H., Dong, P., Li, D., Legant, W.R., Grimm, J.B., Lavis, L.D., Betzig, E., Tjian, R., and Liu, Z. (2016). Real-time imaging of Huntingtin aggregates diverting target search and gene transcription. eLife *5*, e17056.

Love, M.I., Huber, W., and Anders, S. (2014). Moderated estimation of fold change and dispersion for RNA-seq data with DESeq2. Genome Biol. *15*, 550.

Mangiarini, L., Sathasivam, K., Seller, M., Cozens, B., Harper, A., Hetherington, C., Lawton, M., Trottier, Y., Lehrach, H., Davies, S.W., and Bates, G.P. (1996). Exon 1 of the HD gene with an expanded CAG repeat is sufficient to cause a progressive neurological phenotype in transgenic mice. Cell *87*, 493–506.

Mazarei, G., Neal, S.J., Becanovic, K., Luthi-Carter, R., Simpson, E.M., and Leavitt, B.R. (2010). Expression analysis of novel striatal-enriched genes in Huntington disease. Hum. Mol. Genet. *19*, 609–622.

Menalled, L.B., Sison, J.D., Dragatsis, I., Zeitlin, S., and Chesselet, M.-F. (2003). Time course of early motor and neuropathological anomalies in a knock-in mouse model of Huntington's disease with 140 CAG repeats. J. Comp. Neurol. *465*, 11–26.

Menalled, L., El-Khodor, B.F., Patry, M., Suárez-Fariñas, M., Orenstein, S.J., Zahasky, B., Leahy, C., Wheeler, V., Yang, X.W., MacDonald, M., et al. (2009). Systematic behavioral evaluation of Huntington's disease transgenic and knock-in mouse models. Neurobiol. Dis. *35*, 319–336.

Menniti, F.S., Faraci, W.S., and Schmidt, C.J. (2006). Phosphodiesterases in the CNS: targets for drug development. Nat. Rev. Drug Discov. *5*, 660–670.

Park, J.-S., Voitenko, N., Petralia, R.S., Guan, X., Xu, J.-T., Steinberg, J.P., Takamiya, K., Sotnik, A., Kopach, O., Huganir, R.L., and Tao, Y.X. (2009). Persistent inflammation induces GluR2 internalization via NMDA receptor-triggered PKC activation in dorsal horn neurons. J. Neurosci. *29*, 3206–3219.

Plotkin, J.L., and Surmeier, D.J. (2015). Corticostriatal synaptic adaptations in Huntington's disease. Curr. Opin. Neurobiol. *33*, 53–62.

Sadri-Vakili, G., Menon, A.S., Farrell, L.A., Keller-McGandy, C.E., Cantuti-Castelvetri, I., Standaert, D.G., Augood, S.J., Yohrling, G.J., and Cha, J.H. (2006). Huntingtin inclusions do not down-regulate specific genes in the R6/2 Huntington's disease mouse. Eur. J. Neurosci. *23*, 3171–3175.

Shirasaki, D.I., Greiner, E.R., Al-Ramahi, I., Gray, M., Boontheung, P., Geschwind, D.H., Botas, J., Coppola, G., Horvath, S., Loo, J.A., and Yang, X.W. (2012). Network organization of the huntingtin proteomic interactome in mammalian brain. Neuron *75*, 41–57.

Spiteri, E., Konopka, G., Coppola, G., Bomar, J., Oldham, M., Ou, J., Vernes, S.C., Fisher, S.E., Ren, B., and Geschwind, D.H. (2007). Identification of the transcriptional targets of FOXP2, a gene linked to speech and language, in developing human brain. Am. J. Hum. Genet. *81*, 1144–1157.

Sun, W., Cornwell, A., Li, J., Peng, S., Osorio, M.J., Aalling, N., Wang, S., Benraiss, A., Lou, N., Goldman, S.A., and Nedergaard, M. (2017). SOX9 is an astrocyte-specific nuclear marker in the adult brain outside the neurogenic regions. J. Neurosci. *37*, 4493–4507.

Takahashi, K., Liu, F.C., Hirokawa, K., and Takahashi, H. (2003). Expression of Foxp2, a gene involved in speech and language, in the developing and adult striatum. J. Neurosci. Res. *73*, 61–72.

The Huntington's Disease Collaborative Research Group (1993). A novel gene containing a trinucleotide repeat that is expanded and unstable on Huntington's disease chromosomes. Cell *72*, 971–983.

Vernes, S.C., Spiteri, E., Nicod, J., Groszer, M., Taylor, J.M., Davies, K.E., Geschwind, D.H., and Fisher, S.E. (2007). High-throughput analysis of promoter occupancy reveals direct neural targets of FOXP2, a gene mutated in speech and language disorders. Am. J. Hum. Genet. *81*, 1232–1250.

Vernes, S.C., Oliver, P.L., Spiteri, E., Lockstone, H.E., Puliyadi, R., Taylor, J.M., Ho, J., Mombereau, C., Brewer, A., Lowy, E., et al. (2011). Foxp2 regulates gene networks implicated in neurite outgrowth in the developing brain. PLoS Genet. *7*, e1002145.

Yang, J., Seo, J., Nair, R., Han, S., Jang, S., Kim, K., Han, K., Paik, S.K., Choi, J., Lee, S., et al. (2011). DGKι regulates presynaptic release during mGluR-dependent LTD. EMBO J. *30*, 165–180.

Yoo, S.Y., Pennesi, M.E., Weeber, E.J., Xu, B., Atkinson, R., Chen, S., Armstrong, D.L., Wu, S.M., Sweatt, J.D., and Zoghbi, H.Y. (2003). SCA7 knockin mice model human SCA7 and reveal gradual accumulation of mutant ataxin-7 in neurons and abnormalities in short-term plasticity. Neuron *37*, 383–401.

Zuccato, C., Valenza, M., and Cattaneo, E. (2010). Molecular mechanisms and potential therapeutical targets in Huntington's disease. Physiol. Rev. *90*, 905–981.